Pool Boiling Heat Transfer to Cryogenic Liquids;

I. Nucleate Regime Data and a Test of Some Nucleate Boiling Correlations

P. G. KOSKY and D. N. LYON

University of California, Berkeley, California

Pool nucleate boiling heat transfer curves for pure nitrogen, oxygen, argon, methane, and carbon tetrafluoride have been measured on a horizontal, flat, circular, platinum plated disk for saturation pressures ranging from 1 atm. or less to the immediate vicinity of the critical pressure for each liquid. The results have been compared with various suggested nucleate boiling correlations, and the correlations of McNelly, of Kutateladze, and of Borishanskiy-Minchenko are found to be roughly equally successful and all distinctly superior to those of Rohsenow, of Gilmour, and of Forster and his collaborators for these liquids. For oxygen, argon, methane, and carbon tetrafluoride, boiling hysteresis of a type not previously reported was observed at intermediate and high saturation pressures on this surface.

The use of cryogenic liquids in boiling heat transfer studies serves to provide data which are useful in the design of low temperature systems and which may further our understanding of the fundamental boiling phenomena.

We have studied pool boiling heat transfer for pure nitrogen, oxygen, argon, methane, and carbon tetrafluoride, and some nitrogen-oxygen mixtures on a flat, horizontal, platinum plated surface over virtually the entire liquid range for each fluid, covering the full nucleate regime through the peak nucleate boiling flux (hereafter abbreviated to P.N.B.F.). We present here various aspects (*1*) of the nucleate regime heat transfer for these pure liquids and a comparison of these data with the predictions of some of the many correlations which have been proposed for nucleate boiling.

APPARATUS

The apparatus used here was a modification of that used previously (2) and is shown schematically in Figure 1. The test element *A* is submerged in the test liquid near the bottom of the flanged 18-8-type 304 stainless steel pressure vessel (15 cm. diameter × 30 cm. deep). Liquid nitrogen is circulated at a constant rate through the condensing coil *B* located in the vapor space of the pressure vessel.

Two calibrated copper constantan thermocouples *E* and *F*, installed within 2 cm. of the test surface, monitor the bulk liquid temperature. Auxiliary heaters *C* and *D* supplement the test element power so as to exactly compensate the refrigeration introduced through condensing coil *B* and thus to maintain any desired bulk liquid temperature constant (±0.05°K.). Power to auxiliary heater *D* is provided by a proportional controller driven by the error signal from thermocouple *F* and its reference potentiometer; power to auxiliary heater *C* is adjusted manually as necessary.

Tubulations *G* and *G'* are connected to the differential pressure liquid level gauge; *G* also connects to a calibrated 0 to 1,000 lb./sq. in. gauge test gauge. *G* and *G'* also serve as sampling taps for the Beckman model E2 oxygen meter used to analyze the liquid and vapor phases when working with mixtures. A 2.2 cm. O.D. stainless steel tube connects the pressure vessel to a manifold which includes a rupture disk safety valve, a filling port, valves for evacuation, and a small Bourdon gauge. The flange seal for the pressure vessel consists of tongue and groove elements with a pure indium gasket.

Test element *A* provides a flat circular test surface, its heater and thermocouples, and a guard heater. Figure 2 is an exploded view of the test surface-heater unit developed for this work. The polished, platinum plated end of a 1.9 cm. diameter electrolytic tough pitch copper cylinder *J* provides the test surface proper. Two well-tempered copper-constantan thermocouple junctions, *K* and *L*, are located on the axis of *J* approximately 0.18 and 0.89 cm. below the test surface. The end of *J* opposite the test surface is silver soldered to a boss on a 7.5 cm. diameter composite copper disk *O* and *R* which carries the test surface heater (a bifilar helix of resistance wire *Q*), embedded in ceramic *P*. To minimize radial variations in heat flux in the short copper cylinder, a 0.079 cm. thick disk of stainless steel *N* is sandwiched in the silver solder joint between *J* and *O*.

Thermocouples *K* and *L* and the heater leads *Q* are carried outside in the conduit *H*. An Everdur shroud *I* protects the tempering length of thermocouples and is soldered to *J* and *O* to form, together with conduit *H*, a pressure tight compartment for the thermocouples and heater.

To minimize parasitic heat leak from the test element-heater assembly, the guard heater completely surrounds all passive surfaces of the assembly (except where the conduit *H* penetrates the guard heater).

The guard heater is shown schematically in Figure 3. A 0.05 cm. thick cylindrical copper shroud *U* is concentric with *J* and contacts the experimental liquid in the same plane as the test surface. It is silver soldered to a copper top plate *W* with a 0.079 cm. thick stainless steel insert *V* in the same plane as *N*, Figure 2. *W* is soft soldered to a composite copper ring *DD* and *D'D'* which carries a heater *Y* embedded in cement. Heater leads are brought into a recess in the base of ring *DD* by conduit *CC* from outside the cryostat. The conduit and heater cavity were leak tight.

Accurately machined segments of thermal insulation *X* fill the space between the test element-heater assembly and the guard heater so as to expose only the platinum plated test surface and the tip of the guard heater shroud to liquid. Difference thermocouple *AA* is soldered to the base of the test element heater disk *R* (Figure 2) and is held against the copper base plate *EE* of the guard heater by pressure plate *FF* to provide electrically insulated thermal contact. *AA* provides the error signal for the proportional controller which powers the guard heater *Y*.

The guard heater is encased in 1.3 cm. or more thermal insulating material. For early work, silicone resin bonded fiber glass (NEMA grade G-7) was used. Subsequently, when it was suspected that liquid methane was leaching out the silicone resin, this fiber glass was replaced by Teflon.

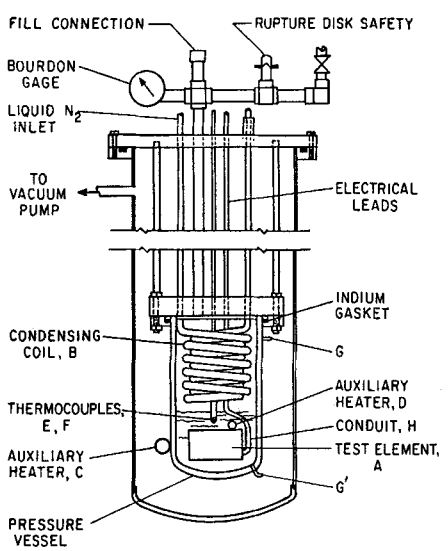

Fig. 1. Experimental cryostat.

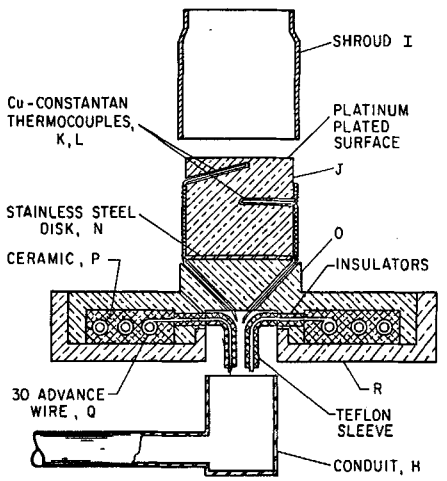

Fig. 2. Exploded view of test element.

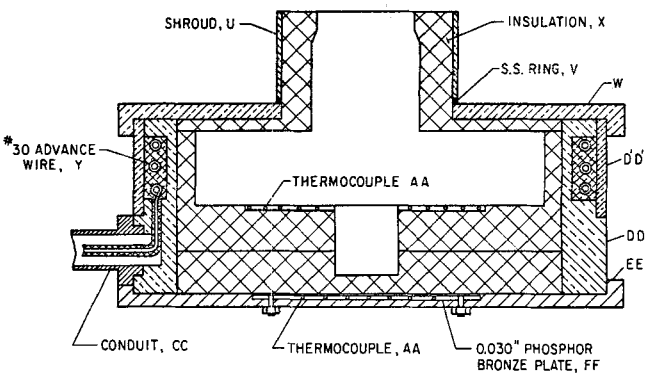

Fig. 3. Construction of guard heater for test element A.

D.C. power with a maximum ripple of 0.015 v. at 150 v. to the test surface heater was measured with calibrated ammeters and voltmeters.

The electromotive forces of thermocouples *E* and of *K* or *L* were compared with precision potentiometers (1μv); the amplified unbalance signals were displayed on a two-channel recorder.

EXPERIMENTAL

Thermocouple Calibration

The thermocouples *E* and *F* were calibrated against approximately forty-eight vapor pressure points pertaining to nitrogen, oxygen, argon, and carbon dioxide. For temperatures greater than 150°K. the interpolations were guided by comparison with the electromotive forces measured in this laboratory for very similar wire which was indirectly compared with the helium gas thermometer from 15° to 300°K. The vapor pressures of the fluids were taken from the compilation of Hilsenrath et al. (3). The triple-point temperature of carbon dioxide was taken from the data of Meyers and Van Dusen (4).

The test element thermocouples *K* and *L* were calibrated against the relevant *E* and *F* thermocouples at zero test element power at each experimental bulk liquid temperature.

The vapor pressure of the liquid was measured by the test gauge (calibrated with a dead weight piston gauge to ± ½ lb./sq.in.). It is estimated that the absolute temperature scale is accurate to 0.1°K.

Surface Preparation and Charging Experimental Vessel

One of the principal aims in this work was to identify the effect of changes in fluid properties as distinct from the tremendous influence of changes in the physical or chemical property of the solid surface upon boiling heat transfer (5, 6). Platinum was chosen in the earlier work (2), and we continued with platinum so that these results would be as comparable as possible with the previous ones. In retrospect, the choice of platinum may have been unfortunate in spite of its reputation for chemical stability, for it is not possible at this time to say that the formation or decomposition of a surface layer of platinum oxides or changes in the surface mobility (7) of adsorbed oxygen cannot be responsible for or contribute to the observed spontaneous changes in boiling heat transfer characteristics, and for the unusual hysteresis effects observed with various fluids for surface temperatures in the 120° to 150°K. region.

Platinum is hard to clean in the ultimate sense (8), but in these tests reproducible rather than clean surfaces were required. Whenever the test element had been exposed to the laboratory atmosphere for any reason, typi-

cally it was washed with reagent grade acetone followed by 95% alcohol, or it was washed with water detergent solution and rinsed with distilled water until an unbroken film could be formed. The platinum was then dabbed dry with a soft paper tissue. The surface would then be heated to ~ 80°C. in a 1-μ vacuum. Success in achieving reproducibility was minimal at best. The exact surface preparation used prior to each run is tabulated in Appendix *B*, reference *1*.

A few parts per million of dissolved solids of low solubility in a boiling liquid can serve to coat and drastically alter with time the boiling heat transfer characteristics of a surface (*6*). In an attempt to strip all high boiling materials from the experimental liquids, they were passed through a cold trap (packed with silica gel) in the line by which they entered the previously evacuated and flushed experimental pressure vessel. Sufficient liquid was added to the pressure vessel to cover the bulk liquid thermocouple tips by 1 to 1½ in.

Physical Properties of the Fluids Investigated

Literature sources for physical property data used are listed in Table 1.

Nitrogen. The nitrogen used had a purity of 99.95 to 99.98%, the principal impurities being oxygen and argon. Any dissolved solids should be very low, probably well below 1 p.p.m. and probably the lowest of any of the fluids investigated.

Oxygen. The oxygen used was 99.5 to 99.8% O_2, with the main impurity argon. It was shown (Run 43, reference *1*) that a small amount of argon (1.8%) in oxygen does not affect nucleate boiling characteristics. Therefore, the physical properties of pure oxygen were used.

Argon. The argon used was 99.99% pure. It was necessary to extrapolate the Ziebland and Burton (*22*) thermal conductivity data to saturated conditions. This extrapolation is probably accurate to ~ 3 to 5%.

Methane. The methane used was Matheson high purity dry 99.95% methane. The principal impurities were stated to be carbon monoxide and air. The latent heat data were extrapolated from 165° to 190°K. The liquid thermal conductivity data of Borokovik et al. (*24*) were used. Discrepancies with the data of Pavlovich (*24*) cast some doubt as to the precision of these data for k.

Carbon Tetrafluoride. DuPont Freon 14 (98.5% carbon tetrafluoride) was used. The main impurities were stated to be air and carbon monoxide. The availability of thermophysical property data for carbon tetrafluoride was the poorest of the materials studied. The liquid density data of Knobler and Pings (*15*) are the best available; however, the DuPont liquid density data (*10*) are presumably internally consistent with their vapor pressure-temperature scale and were used for that reason. The saturated liquid phase specific heat was obtained from

$$C_{sat} = \left(\frac{\partial H}{\partial T}\right)_{sat} - V\left(\frac{\partial P}{\partial T}\right)_{sat} \qquad (1)$$

in which $(\partial H/\partial T)_{sat}$ was obtained by graphically differentiating a plot of the DuPont saturated liquid enthalpy vs. absolute temperature data. Only one liquid thermal conductivity measurement was available for carbon tetrafluoride (at 160°K.). From this the whole temperature range was predicted from the correlation given by Bird, Stewart, and Lightfoot (*25*). No viscosity measurements were available, and the formula of Eyring (*26*) was used together with a generalized correlation (*27*) to predict values over the complete liquid range. Obviously, large uncertainties in the fluid property values used for carbon tetrafluoride pertain, particularly at higher pressures.

Table 1. Fluid Thermophysical Property Data Sources

Property	Source reference for N_2	O_2	Ar	CH_4	CF_4
P	*3*	*3*	*3*	*9*	*10*
ρ_l, ρ_v	*11, 12*	*13*	*14*	*9*	*10*
λ	*16*	*16*	*16*	*9*	*10*
C_l	*17*	*17*	*17*	*17*	*10*
σ	*18*	*19*	*18*	*20*	*21*
k	*23*	*22*	*23*	*24*	*25*
μ	*28*	*28*	*17*	*28*	*26, 27*

Heat Transfer Measurements

The normal mode of operation was to increase the flux from the immediate prior point. At low fluxes the increments were ~ 5 w./sq.cm. decreasing to ~ 1/3 w./sq.cm. as the P.N.B.F. was approached. Occasional curves were taken by starting at a flux slightly below the P.N.B.F. and then decreasing the flux step-by-step to identify the extent of hysteresis between ascending and descending flux curves for a given surface. Upon completion of an isobar, the bath thermocouple reference potentiometer was reset to a higher temperature and a new isobar completed. The sequence was repeated until the critical pressure was approached.

Check data were taken at the end of each run by repeating the thermodynamic conditions of the initial isobar and retaking the complete nucleate curve to the P.N.B.F.

Determination of the Parasitic Heat Leak Correction

A solid nylon disk was placed over the test element surface and held against it by a spring-loaded clamp. With the covered test surface immersed in nitrogen, the power input to the test element heater necessary to maintain ΔT's up to 30°K. between the test element and the bulk liquid was measured at various bath temperatures. By correcting for the heat flow through the nylon cap, the parasitic heat loss from the test element (probably mainly along the conduit H) was determined. It could be represented at all bath temperatures to within 10% by

$$\delta(Q/A) = 0.0046\ (T_{av} - T)\ \text{w./sq.cm. of test surface} \qquad (2)$$

It amounted to roughly 1% of the total input to the test element heaters under all conditions.

Determination of the Test Surface Temperature

To within the maximum uncertainty in the location of the tips of K and L, the experimental thermal conductivity for J agreed with literature values for E.T.P. copper (*12*). The temperature drop between the uppermost thermocouple, and the test surface is given by

$$\delta T = \frac{0.183}{k}(Q/A) \quad °K. \qquad (3)$$

or

$$\delta T = 0.041\ (Q/A) \quad °K. \qquad (4)$$

for a test element temperature of 100°K. The extreme limits of uncertainty in this temperature drop are estimated at ± 30%. The effect of this uncertainty upon the extreme limit of uncertainty in ΔT or $(T_{surface} - T_{liquid})$ varies from less than 1% at low fluxes at low pressures to almost 25% for nitrogen at the P.N.B.F. at a saturation pressure of 23 atm. in the worst case.

EXPERIMENTAL RESULTS

The complete nucleate boiling data and the P.N.B.F. data are listed in Appendix *B* of Kosky (*1*). We present here representative samples of those data. The estimated accuracy of the various quantities listed due to random errors are

Q/A, ± 1% at fluxes in excess of ~ 10 w./sq.cm.
ΔT, ± 0.05°K.
T, ± 0.05°K.

At lower fluxes the uncertainties in Q/A were perhaps twice as large.

Systematic errors are of the following order of magnitude:

A, ± 0.2%
ΔT, ± 0.025 Q/A °K. (extreme limit due to uncertainty in the location of the thermocouple tip)
T, ± 0.1°K.

Selected nucleate boiling curves are shown in Figures 4 through 12, inclusive.

Figure 4 is a plot of Q/A vs. ΔT for nitrogen from Run 46 at pressures ranging from 1.09 to 32.4 atm. (obtained in a continuous sequence of measurements on a single charge of liquid).

As has been observed and reported before (*29, 5, 6*), the decreasing flux boiling curves often lie significantly above the curve obtained by increasing the heat flux. Figure 5 is an extreme example of such hysteresis obtained during the first measurements with nitrogen on the initial plated surface of this test element. No significant hysteresis was observed with oxygen when the nitrogen was removed and the vessel charged with oxygen without exposing the surface to the laboratory atmosphere, nor with nitrogen following polishing and replating of the surface. Figures 4 and 5 indicate the variation in performance of two ostensibly identical samples of the same surface prepared by repeating the same procedures. The replated surface would sustain a 2.5 to 3°K. superheat before nucleation when increasing the flux from zero (3.53 atm. isobar, Figure 6). After nucleation, the ascending and descending curves were essentially coincident for the replated surface.

Figure 6 illustrates the change in heat transfer characteristics with time for a given surface that can occur even though the same preparative procedures have been used. It also illustrates that check data should be taken at low rather than high pressures.

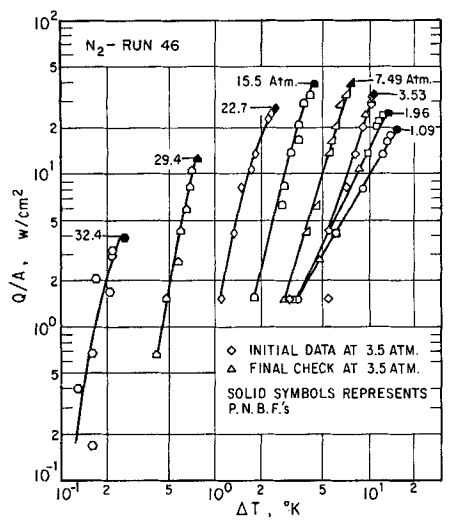

Fig. 4. Nucleate boiling curves for nitrogen on horizontal platinum.

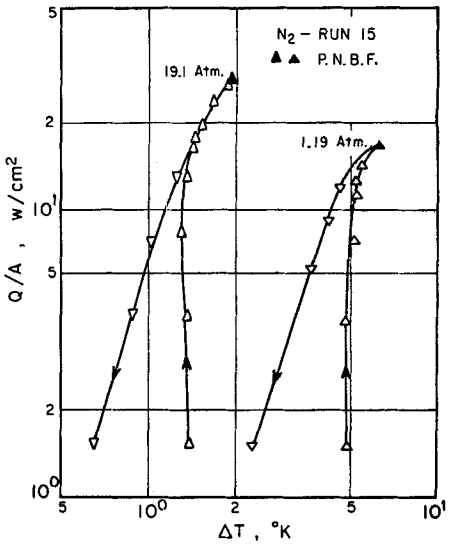

Fig. 5. Extreme example of hysteresis in nucleate boiling of nitrogen on platinum.

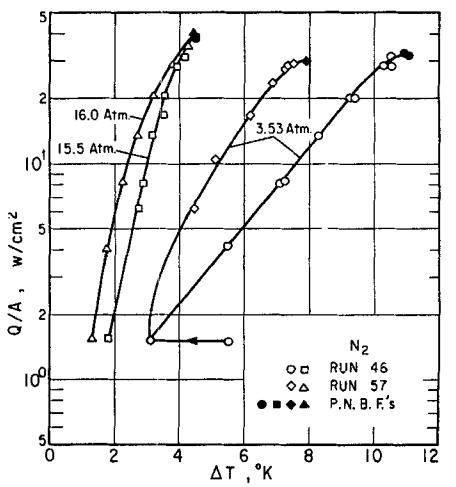

Fig. 6. Variation in the nucleate boiling characteristics of nitrogen on a given platinum surface.

Figure 7 shows a consistent set of isobars for oxygen ranging from 0.25 to 48.4 atm. 1.02 atm. check data indicated reproducibility to ± 2% over the duration of this run. Therefore, the drastic change in the character of the (Q/A) vs. ΔT curves for oxygen on this surface between 8 and 16 atm. is real. In addition a new type of severe hysteresis occurs between 8 and 16 atm. Figure 8 of 9.9 atm. isobars is typical of this regime and pressure region. We strongly suspect that this behavior was responsible for the anomalous oxygen results reported earlier (2), rather than film boiling over a small segment of the platinum foil as postulated then.

Figure 9 gives a consistent set of curves for argon as indicated by the three 1.07 atm. isobars. Five isobars were measured prior to those plotted. During an excursion into film boiling in the course of P.N.B.F. determinations on the fifth isobar at 8.4 atm., the heat transfer characteristics of the surface changed abruptly but remained constant thereafter at the new values. Again, at pressures in the vicinity of and above 16 atm., argon, like oxygen above 8 atm., exhibits inverted hysteresis loops at high fluxes. The reproducibility of this hysteresis is indicated by the two isobars at 32.9 atm. (Runs 48-10 and 48-12) plotted in Figure 9. An isobar at 1.06 atm. was measured between the two. Four additional isobars were omitted from Figure 9 for clarity.

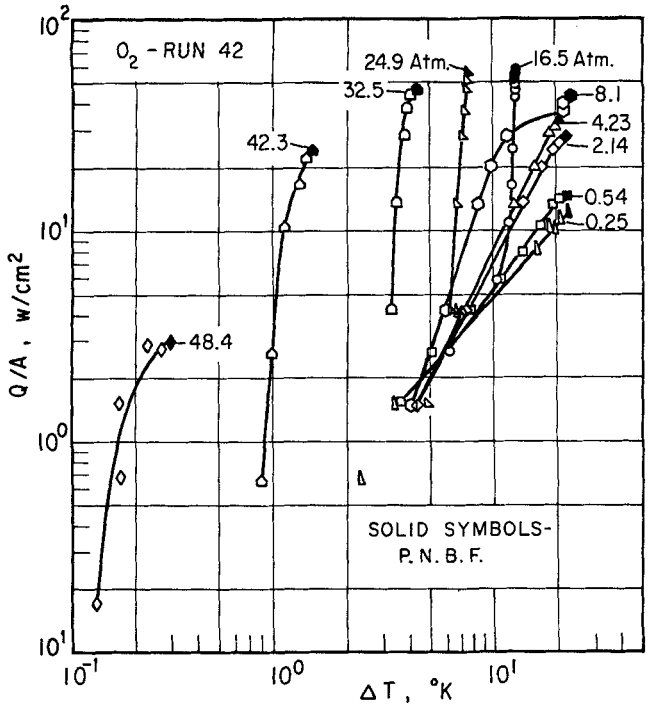

Fig. 7. Nucleate boiling curves for oxygen on horizontal platinum.

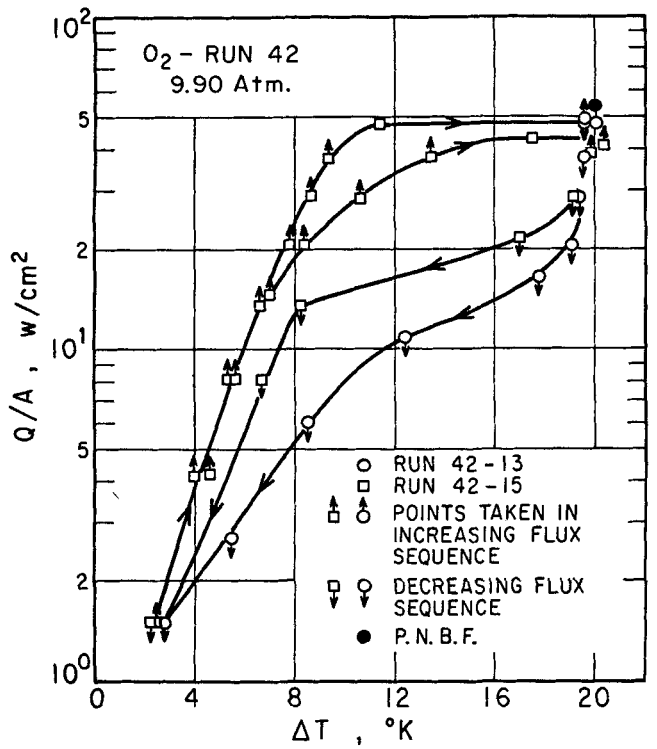

Fig. 8. Hysteresis in nucleate boiling of oxygen on platinum at 9.9 atm.

Of the liquids tested, the reproducibility of data was poorest for methane (see the two 1.07 atm. check runs in Figure 10). (For clarity, five isobars have been omitted.) Silicone resin leached from the fiber glass insulation and deposited on the test surface cannot explain this lack of reproducibility. Similar results were obtained following rigorous cleaning of the pressure vessel and replacement of all fiber glass insulation with Teflon. We suspect the poor reproducibility is associated with the extreme difficulty of freeing methane from impurities which adsorb at solid surfaces (*20*) and drastically alter wetting (and boiling) characteristics (*30, 31*).

At intermediate pressures the curves are characterized by instabilities and at high pressures by hysteresis loops similar to those in oxygen and argon.

Figure 11 shows three isobars selected from the nine of Run 58 with carbon tetrafluoride. Again, hysteresis loops at pressures above 16 atm. and poor reproducibility (see 1.01 atm. check runs) characterize the data.

Both the carbon tetrafluoride and methane agree with the reported behavior of higher boiling organic liquids (*32, 33*) in that n, in the relationship $(Q/A) = b(\Delta T)^n$, decreases as the critical pressure is approached in contrast with nitrogen, oxygen, and argon, where we find that n increases.

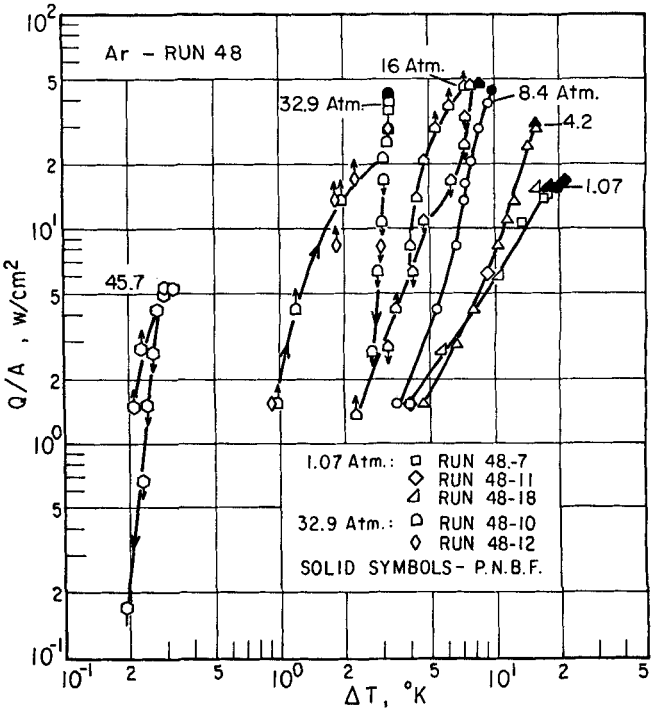

Fig. 9. Nucleate boiling curves for argin on horizontal platinum.

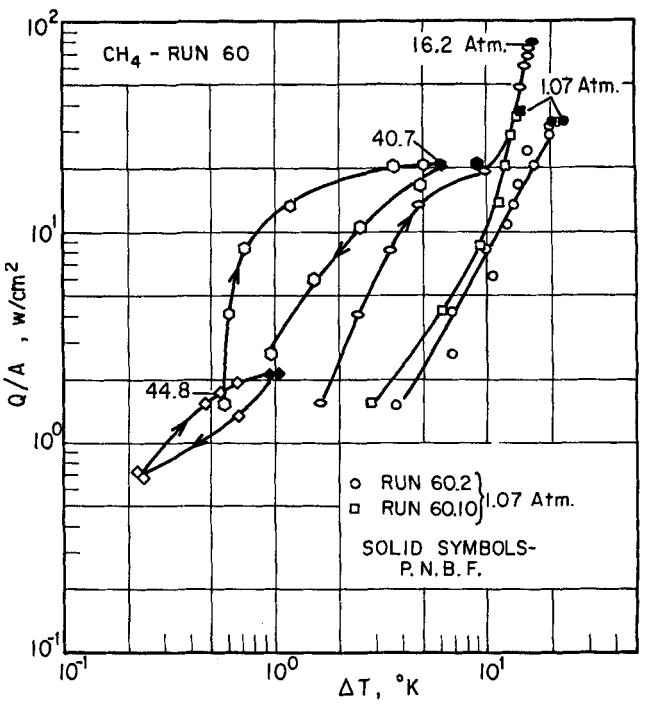

Fig. 10. Selected nucleate boiling curves for methane on horizontal platinum.

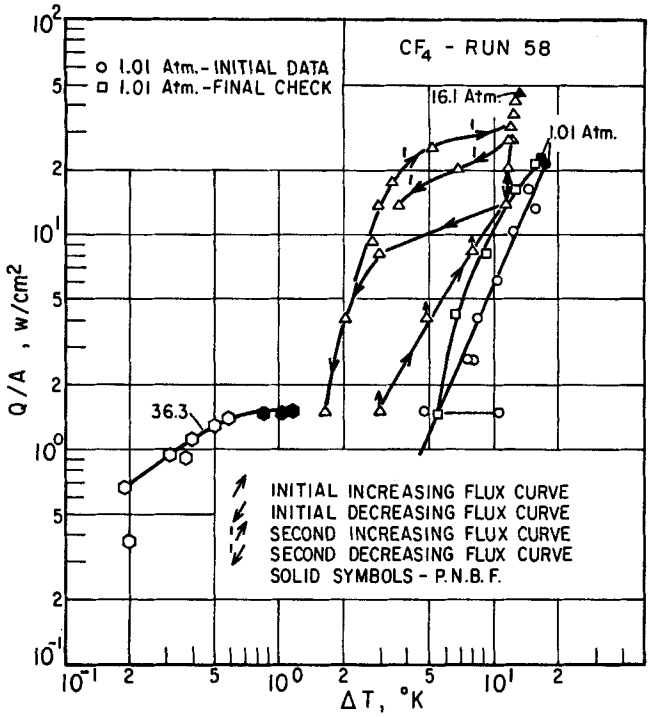

Fig. 11. Selected nucleate boiling curves for carbon tetrafluoride on horizontal platinum.

COMPARISON OF RESULTS WITH NUCLEATE BOILING CORRELATIONS

A large number of empirical or semiempirical correlations have been proposed for the nucleate boiling regime. Some, for example, those of Tien (*34*) and of Lienhard (*35*), include parameters related to the number of nucleating sites per unit area as well as to fluid properties in an attempt to accommodate the tremendous influence of surface conditions. We have not attempted to relate our data to such correlations, since we had no independent way of determining the number of active sites at any time, nor were we confident that the potential site population for our surfaces remained constant so that we could compare different fluids on the same surface to test the validity of the correlations.

Most nucleate boiling correlations may be expressed in the form

$$\Pi_0 = K_{sf}\,\Pi_1^{n_1}\,\Pi_2^{n_2} \ldots\ldots \quad (5)$$

where Π_0, Π_1, Π_2, ... are dimensionless groups containing (Q/A), ΔT, and various thermophysical properties of the fluids. The surface-fluid interaction parameter K_{sf} and the exponents n_1, n_2, ... are fitted from data. Except for Rohsenow's (*36*) correlation, a single K_{sf} is assumed to hold for all fluid-solid pairs.

We have arbitrarily selected several correlations expressed in the form of Equation (5) and have tested how well they account for the fluid property dependence of boiling heat transfer to cryogenic liquids. We chose the correlations of Rohsenow (*36*), Forster-Zuber (*37*), Forster-Greif (*38*), Gilmour (*39*), McNelly (*40*), Kutateladze (*41*), and Borishanskiy-Minchenko (*41b*) [Equations (6) to (11), respectively].

$$\frac{C_l\Delta T}{\lambda} = K_{sf}\left[\frac{Q/A}{\mu\,\lambda}\left(\frac{\sigma}{g(\rho_l-\rho_v)}\right)^{1/2}\right]^{0.33}\left[\frac{C_\mu}{k}\right]_l^{1.7} \quad (6)$$

$$\frac{Q/A}{\lambda\rho_v}\left(\frac{C_l\rho_l\sqrt{\pi\alpha}}{k}\sqrt{\frac{2\sigma}{\Delta P}}^{4}\sqrt{\frac{\rho_l}{\Delta P}}\right)$$

$$= 0.0015\left[\frac{\rho_l}{\mu}\left(\frac{\Delta T\,C_l\rho_l\sqrt{\pi\alpha}}{\lambda\rho_v}\right)^2\right]^{0.62}\left[\frac{C_\mu}{k}\right]_l^{0.33} \quad (7)$$

$$\frac{\lambda\rho_v}{C_l\rho_l\Delta T} = 0.001\left(\frac{\rho_l D\;Q/A}{\mu\lambda\rho_v}\right)^{-0.3}\left(\frac{P^2}{\rho_l g\,\sigma}\right)^{0.425}\left(\frac{C_\mu}{k}\right)_l^{-0.6} \quad (8)$$

$$\frac{hD}{k} = 0.225\left(\frac{D\;Q/A}{\lambda\mu}\right)^{0.69}\left(\frac{PD}{\sigma}\right)^{0.31}\left(\frac{\rho_l}{\rho_v}-1\right)^{0.33}\left(\frac{C_\mu}{k}\right)_l^{0.69} \quad (9)$$

$$\frac{h}{k}\left(\frac{\sigma}{g(\rho_l-\rho_v)}\right)^{1/2} = 7.0\times10^{-4}\left[\frac{Q/A}{\alpha\rho_v\lambda}\left(\frac{\sigma}{g(\rho_l-\rho_v)}\right)^{1/2}\right]^{0.7}\left[\frac{P}{\sigma}\left(\frac{\sigma}{g(\rho_l-\rho_v)}\right)^{1/2}\right]^{0.7}\left[\frac{C_\mu}{k}\right]_l^{-0.35} \quad (10)$$

$$\frac{h}{k}\left(\frac{\sigma}{g(\rho_l-\rho_v)}\right)^{1/2} = 8.7\times10^{-4}\left[\frac{Q/A}{\alpha\rho_v\lambda}\left(\frac{\sigma}{g(\rho_l-\rho_v)}\right)^{1/2}\right]^{0.7}\left[\frac{P}{\sigma}\left(\frac{\sigma}{g(\rho_l-\rho_v)}\right)^{1/2}\right]^{0.7} \quad (11)$$

The literature contains many other correlations. Drayer (*42*) and Zuber and Fried (*43*) list eleven and seven correlations, respectively, and have used them for cryogenic fluids. Rohsenow indicates different values of K_{sf} ranging between 0.0025 and 0.013 for various fluid-solid combinations. We arbitrarily chose a single value of 0.013. The choice of any other value would merely translate the curves of Equation (6) on a log-log plot horizontally by a uniform amount.

We used a single expression [Equation (7)] for both the Forster-Zuber and Forster-Greif correlations. If the exact Clausius-Clapeyron equation is substituted instead of the approximate form used by Forster and Greif, the two equations become identical. Since much of this work was done in regions where the saturation pressure increases so rapidly with temperature that $\Delta T\left(\frac{dp}{dT}\right)_{T\,\text{bulk}}$ gives a poor approximation to ΔP, ΔP was obtained from the actual vapor pressure-temperature relationship of the fluid in comparing our data with Equation (7).

All experimental data for the various fluids were compared with Equations (6) through (11). We present in Figures 12 through 17 the resulting plots of the nitrogen data of Figure 4. The conclusion, drawn from inspection of Figures 12 to 17, that the Gilmour, McNelly, Kutateladze, and Borishanskiy-Minchenko correlations are all superior to the Rohsenow and Forster-Zuber/Forster-Greif correlations is supported by the data on the other fluids with the following exceptions: (1). This degree of success for the Gilmour correlation holds only for nitrogen as is illustrated by Figure 18 which plots the oxygen data of Figure 7 in accordance with Equation (8). (The order of success for the Gilmour correlation was N_2>Ar>O_2>CH_4>CF_4.) (2). The Forster-Zuber/Forster-Greif correlation was roughly as successful for the methane and carbon tetrafluoride data as any correlation tested here, but it must be emphasized that those data are the poorest obtained here.

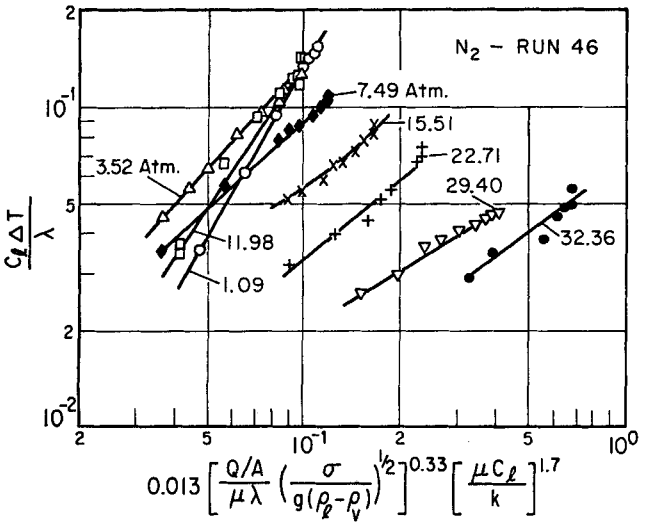

Fig. 12. Rohsenow correlation plot for nitrogen on horizontal platinum.

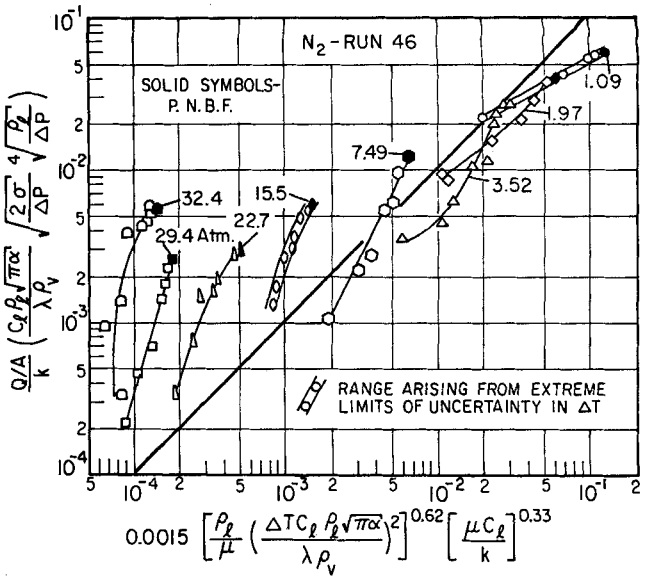

Fig. 13. Forster-Zuber/Forster-Greif correlation plot for nitrogen on horizontal platinum.

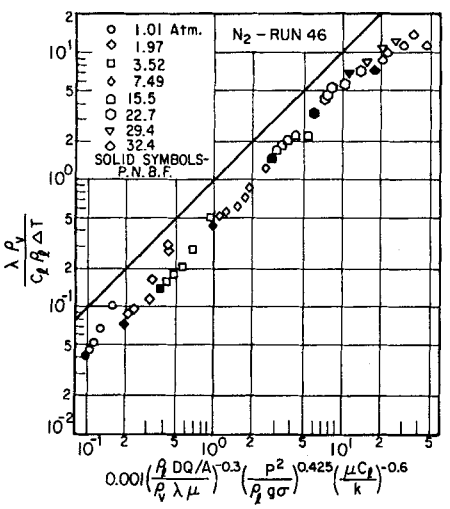

Fig. 14. Gilmour correlation plot for nitrogen on horizontal platinum.

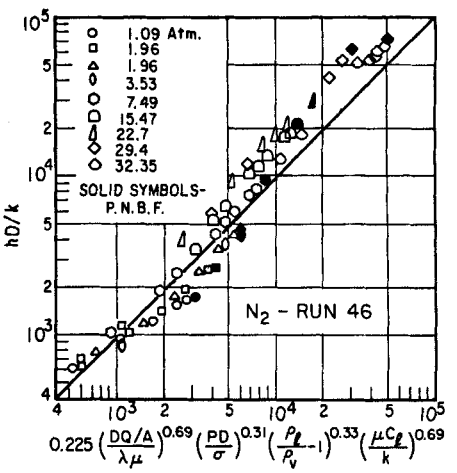

Fig. 15. McNelly correlation plot for nitrogen on horizontal platinum.

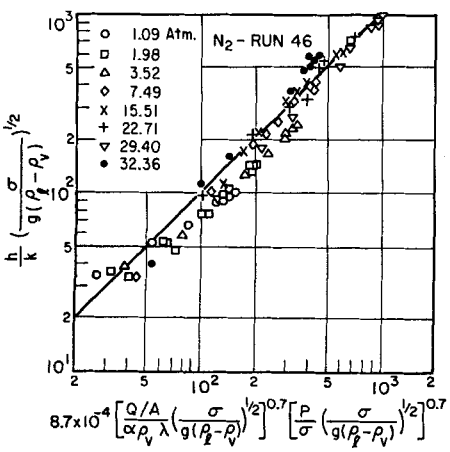

Fig. 16. Borishanskiy-Minchenko correlation plot for nitrogen on horizontal platinum.

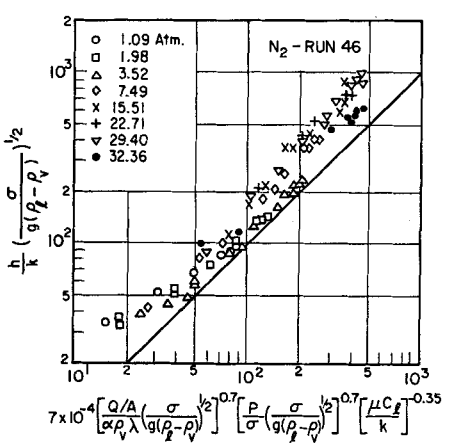

Fig. 17. Kutateladze correlation plot for nitrogen on horizontal platinum.

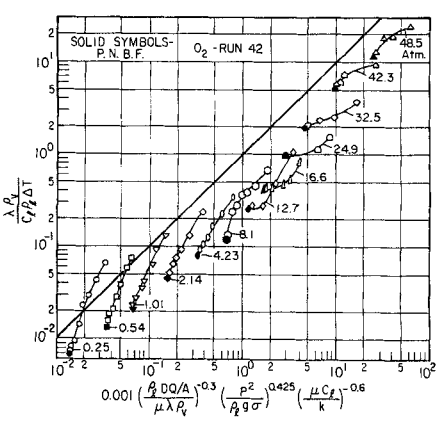

Fig. 18. Gilmour correlation plot for oxygen on horizontal platinum.

DISCUSSION

The magnitude of the systematic, pressure dependent error in ΔT due to uncertainty in the location of the junctions of thermocouples K and L has a negligible effect on testing the correlations. Figure 13 shows the extreme limits of uncertainty ascribable to this error. They fall, in most cases, within the dimensions of the symbol used in plotting.

Except for the inverted hysteresis observed at intermediate pressures here for oxygen, argon, methane, and carbon tetrafluoride, these data show no striking deviations from literature data which cannot be ascribed to variations in the physical texture of the surface. We know of no other data for oxygen taken at intermediate and high pressures which would have revealed the type of hysteresis found here.

The limited range of the 1 atm. data for argon of Bewilogua et al. (*44*) precludes significant comparison with these data. The 1 atm. argon data on horizontal 0.008 in. diameter platinum wire of Bochirol et al. (*45*) are comparable to these except that their P.N.B.F. was ~ 45% of ours. We know of no other existing boiling data with argon or with carbon tetrafluoride.

Park (*46*) investigated methane on a horizontal gold cylinder. His lower P.N.B.F.'s are consistent with the use of a horizontal cylinder vs. flat disk. Park's heater could not deliver enough power to reach the region where we found inverted hysteresis.

The methane data of Sciane et al. (*47*), which covers the full range of flux and pressure, became available during revision of this manuscript. Their lower P.N.B.F.'s are consistent with the use of a horizontal cylinder. They mention no hysteresis at high pressures on their gold surface. The differences in ΔT and in the slope of Q/A vs. ΔT between our data, the data of Park, and the data of Sciance et al. fall within the range of variation that we found from sample to sample of the same surface.

The Borishanskiy-Minchenko correlation [Equation (11)] differs from Kutateladze's [Equation (10)] only in the omission of a Prandtl number term (and the value of K_{sf}), yet they are about equally successful for these fluids. The range of Prandtl numbers for these fluids (~ 1 to 10) is too small for this to represent a significant test of the role of the Prandtl number.

Lienhard (*48*) suggests that the failure at high pressures of the Forster-Zuber/Forster-Greif correlation stems from its incorporation of the empirical relation

$$(\partial \ln \Delta T/\partial \ln p)_Q = - \text{constant} \qquad (12)$$

which is valid only at low pressures.

One would expect that the successful correlations [Equations (9), (10), and (11)] could be improved by using a single experimental datum point for a particular surface to evaluate K_{sf}. However, we found K_{sf} to vary sufficiently from run to run for the same fluid on the same surface, so that this procedure would give improvement over the literature values for K_{sf} only for surfaces whose constancy could be better controlled than we could achieve here.

Figures 12 to 18 can give an exaggerated picture of the utility of these correlations in predicting a boiling curve. The exponent n in $(Q/A) = b(\Delta T)^n$ can vary from ~ 2 to 3.5 for a given situation, so that one can obtain a poor estimate of Q/A corresponding to an assumed ΔT. The P.N.B.F. is well predicted from available correlations (see Part II), so that a more logical approach is to assume a series of fluxes up to this value and calculate the corresponding ΔT's. Such a calculation is shown in Figure 19, where the ratio of a predicted to experimental heat transfer coefficient is plotted vs. Q/A reduced by the P.N.B.F. In addition to Equations (6) to (11), Equation (13) due to Kutateladze (*41a*) is also shown in Figure 19 as it was found superior for cryogens by Brentari et al. (*49*) in 1963:

$$\frac{h(\sigma/g\rho_l)^{1/2}}{k} = 3.25 \times 10^{-4}\left[\frac{Q/A}{\alpha\rho_v\lambda}\left(\frac{\sigma}{g\rho_l}\right)^{1/2}\right]^{0.6} \times \left[\frac{P}{\sigma}\left(\frac{\sigma}{g\rho_l}\right)^{1/2}\right]^{0.7}\left[g\left(\frac{\rho_l}{\mu_l}\right)^2\left(\frac{\sigma}{g\rho_l}\right)^{1.5}\right]^{0.125} \qquad (13)$$

The McNelly, Kutateladze, and Borishanskiy-Minchenko correlations are still clearly superior, but their superiority appears less pronounced when plotted in this way.

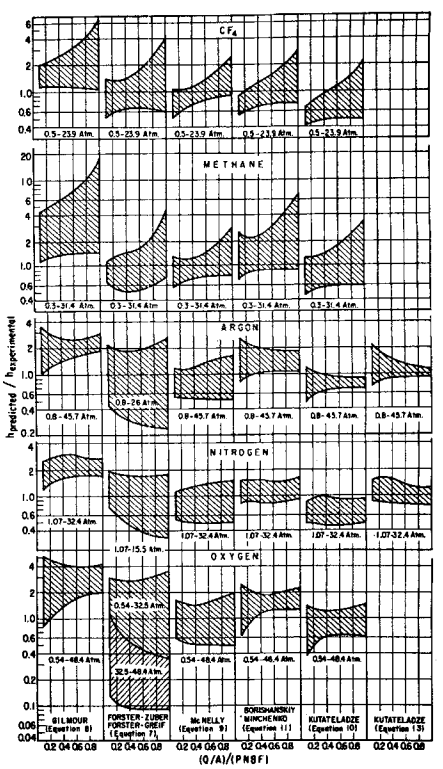

Fig. 19. Ratio of heat transfer coefficient predicted by various correlations to experimentally observed heat transfer coefficients for various fluids vs. fraction of P.N.B.F. (Envelopes of curves for various isobars shown.)

In the absence of information as to the specific site distribution we recommend either the McNelly or Borishanskiy-Minchenko correlation coupled with a prediction of the P.N.B.F. as a means of estimating a nucleate boiling curve for a particular cryogen.

ACKNOWLEDGMENT

We are indebted to J. D. Elson and his staff of mechanicians for their suggestions and skill in designing and assembling the experimental apparatus. We also thank Professor J. H. Lienhard for pointing out the probable cause of failure of the Forster-Greif correlation.